Scale effect and error analysis of crop LAI inversion

ZHU Xiaohua[1, 2], FENG Xiaoming[3], ZHAO Yingshi[2], SONG Xiaoning[2]

1. *Institute of Remote Sensing Applications, Chinese Academy of Sciences, Beijing* 100101, *China*;
2. *Graduate School of the Chinese Academy of Sciences, Beijing* 100049, *China*;
3. *State Key Laboratory of Urban and Regional Ecology, Research Center for Eco-Environmental Sciences, Chinese Academy of Sciences, Beijing* 100085, *China*

Abstract: Leaf area index (LAI) is an important bio-physical character of vegetation and can be effectively achieved through remote sensing technology. However the LAI inversion from low resolution data induces a scaling bias due to the heterogeneous of the surface and model non-linearity, which may cause the scale effect on the LAI estimate. In this work, the Yingke oasis of Heihe River is selected as the study area. Based on Hyperion data, a two-layer canopy reflectance model (ACRM) is introduced to calculate LAI. The low resolution LAI are then achieved in two ways: LAI_{mean}, the mean of LAI, is directly calculated from Hyperion; and the LAI_p is computed from linear cumulative Hyperion data. Statistics shows that there is a serious underestimation of LAI_p. On the basis of LAI-NDVI regresion equation, the Taylor Mean Value Theorem is applied to creat an error factor and to conduct scaling error correction. The result of error correction (LAI_r) has a high relationship with LAI_{mean}, which shows that the method is effective and suitable for scale effect correction and can be used to correct other LAI product, such as MODIS LAI. Finally, the causes for scaling bias are discussed. It is found that the spatial heterogeneous is the key factor which may lead to the error in LAI inversion.

Key words: Hyperion, leaf area index, scale effect, inversion, error correction

CLC number: TP751.1 **Document code:** A

Citation format: Zhu X H, Feng X M, Zhao Y S and Song X N. 2010. Scale effect and error analysis of crop LAI inversion. *Journal of Remote Sensing*. **14**(3): 579—592

1 INTRODUCTION

Leaf area index (LAI) is an important bio-physical character of vegetation, and the scale effect of LAI inversion through remote sensing technology has attracted much concern in recent years. Tian *et al*. (2002, 2003) had conducted a multi-scale analysis of the MODIS LAI product, and presented a method for the MODIS LAI calibration based on the field sampling strategy. They pointed out that when the scale increased, a large number of vegetation types were mixed together, which will cause errors in the LAI inversion. Garrigues *et al.* (2006) used NDVI, R, and NIR to establish semi-empirical models based on single variable and pairs of variables, and then they analyzed the scale effect of LAI inversion and corrected the errors of multi-resolution inversion. After an uncertainty analysis of LAI retrieved from a spatially heterogeneous scene, Yao *et al.* (2007) pointed out that different components of the mixed pixels had great impact on LAI inversion. Zhang *et al.* (2008) had proposed an up-scale conversion method based on NDVI pixel decomposition. However, the research did not discuss the inherent mechanism of scale effect. Xu *et al.* (2009) established LAI conversion formula among different scales based on crop canopy reflectance model. All of these studies point out that scale effect widely exists in LAI retrieval with remote sensing data of different spatial resolutions.

In this paper, the Yingke oasis of Heihe River is selected as the study area. Based on Hyperion data, a two-layer canopy reflectance model (ACRM) is introduced to calculate LAI. Remote sensing data of different resolutions are obtained by linear accumulation method. Based on LAI-NDVI regression equation, Taylor's mean value theorem is introduced to correct the errors of LAI retrieved from low resolution data and realize the large-scale LAI calibration.

2 STUDY AREA AND MATERIALS

2.1 Description of the study area

Heihe is originated in Qilian County, Qinghai Province, situated in the middle of Qilian and Hexi Corridor, bordered with Mongolia Province in the north, connected with Wuwei Basin in the east, and adjacent to Shule River Basin in the west. Heihe Basin is the second largest inland river basin in north-

Received: 2009-07-13; **Accepted**: 2009-10-26

Foundation: National Basic Research Program of China (973 Program, No. 2007CB714407); National Natural Science Foundation (No. 40801070).

First author biography: ZHU Xiaohua (1986—), female, PhD Candidate. Graduated from the Department of Information Management, China Agricultural University, mainly engaged in Quantitative Remote Sensing Application Research. E-mail: zhuxh0118@163.com

Corresponding author: FENG Xiaoming, E-mail: fengxm@rcees.ac.cn

west China, covering an area of 142900km^2. The average annual precipitation is low, be coupled with the impact of human activities, the vegetation cover in this area is inhomogeneous and varied seasonally. The study site in this paper is located in the Yingke oasis of Heihe River where the main vegetations are crops such as wheat and corn (Fig. 1).

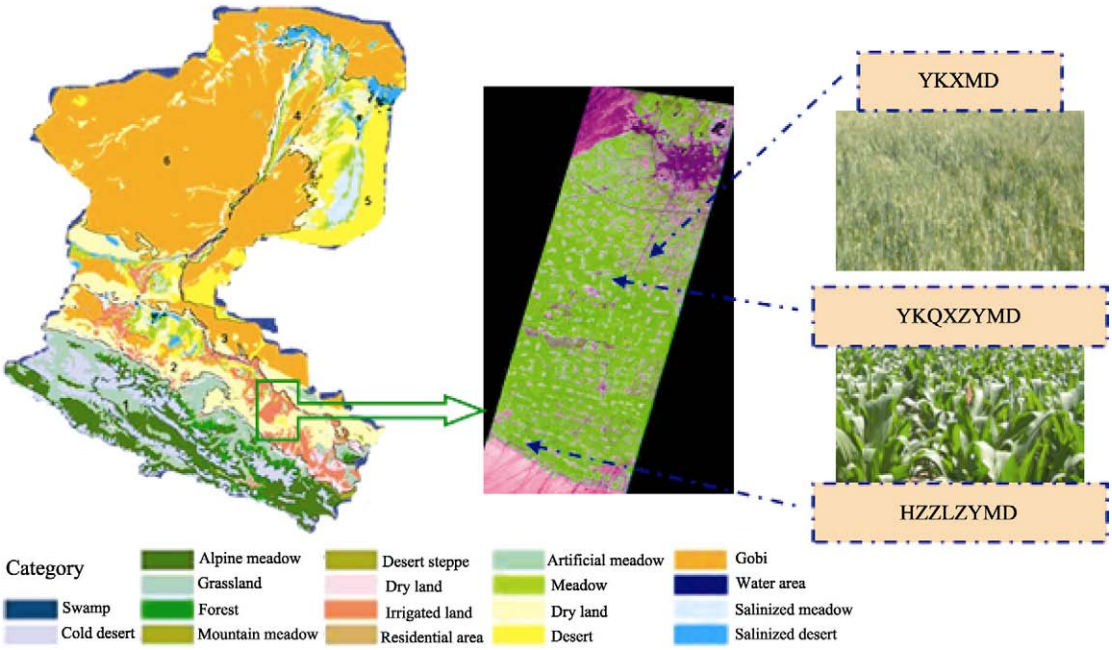

Fig. 1 Location of the study area

2.2 Data preprocess

2.2.1 *Description of the data*

Hyperion data of July 15, 2008 in the Yingke oasis of Heihe River is used in this study. Hyperion is one of the three kinds of sensors in the Earth Observation Satellite (EO-1) which launched on November 21, 2000 by National Aeronautics and Space Administration (NASA). The Hyperion is a push-broom instrument, providing a hyper-spectral image capable of resolving 242 spectral bands (VNIR400—1000nm, SWIR, 900—2500nm) with a 30m spatial resolution. The corresponding filed data is collected from June 13 to June 26, 2008, with crop LAI relatively stable in this period. Samples leaves' lengths and widths were measured both with manual work and LAI-2000, LAI-3000 instruments. Correction factors for each crop were calculated by comparing the manual measured value and the instrument one. Crop LAIs were finally gotten by length and width of crop leaf multiplied by the correction factors.

2.2.2 *Data preprocess*

In this study, atmospheric correction of Hyperion is achieved with FLAASH model. Geometric correction of Hyperion data is conducted with the image-to-image registration method combined with a LANDSAT ETM data. During the correction, the spatial error is controlled under 0.5 pixels. The geometric projection of the image is UTM projection after the correction.

The relatively high correlation between Hyperion bands is widely recognized. Therefore, a reduction in band number without significant information loss (Luo, 2002) is carried out under the principle of larger standard deviation and smaller correlation coefficient. The process of band selection is followed as: (1) remove the bands of small standard deviation; (2) the residual bands are divided into five groups according to the wavelength such as blue band, green band, red band, NIR, SWIR, then seven bands of larger standard deviation are selected in each group; (3) less correlative bands are selected after correlation analysis of bands in each group. Finally, 14 spectral bands are identified for this study (Table 1).

Table 1 Hyperion bands selection for this study

No.	Hyperion band	Wavelength/nm
1	14	487.87
2	18	528.57
3	21	559.09
4	23	579.45
5	26	609.97
6	34	691.37
7	37	721.90
8	40	752.43
9	50	854.18
10	54	894.88
11	83	972.99
12	88	1023.40
13	92	1063.79
14	96	1104.18

3 LAI INVERSIONS

The crops present horizontally uniform distribution in the maturity stage, as shown in Fig. 1. A two-layer canopy reflectance model (Kuusk, 2001) is introduced to calculate LAI. The ACRM model contains PROSPECT leaf optical model (Jacquemoud & Baret, 1990), simulating the reflectance and transmittance of leaf from 400nm to 2500nm through the function relationship of the leaf structure parameters and biochemical parameters. The model can well explain the specula reflection on leaf surface and the "hot spot" phenomenon, and also has a high computational efficiency. The calculation of multiple scattering in the model is same to SAIL model (Verhoef, 1984). This model is a one-dimensional bidirectional turbid medium radiative transfer model that has been later modified to take into account the hot spot effect in plant canopy reflectance (Kuusk, 1985). Turbid medium defines the canopy as a horizontally homogenous and semi-infinite layer that consists of small vegetation elements that act as absorbing and scattering particles of a given geometry and density. Consequently, the model is best adopted for use in homogeneous vegetation canopies (Verhoef, 1984; Feng & Zhao, 2005).

Hyperion image and NDVI data of July 15, 2008 in the Yingke oasis of Heihe are shown in the Fig. 2. Before LAI inversion, the input parameters (such as leaf area index, leaf size parameters, chlorophyll content, soil parameters, etc.) of the ACRM model are set up according to the ground truth data. Fig. 2(c) is the iterative inversion results, and verified by the ground-measured LAI data (Fig. 3). The histogram of the relative error shows that LAI retrieved and LAI measured have a good consistency, with correlation coefficient of 0.79 and RMSE of 0.336. The validation results show that the LAI inversion based on ACRM model is effective, reflecting the conditions on the ground, and can be used for further analysis.

4 QUANTITATIVE ANALYSIS OF SCALE EFFECT

The ACRM model is used for getting LAI value of the study area, while the main purpose of this paper is to study the scale effect of crop LAI, analyzing the source of scale effect and correcting the scaling errors. In order to reduce the impact of the extrinsic factors when retrieving LAI from different resolution data, multi-scale remote sensing data are obtained through linear aggregation of Hyperion 30m reflectance data, and then

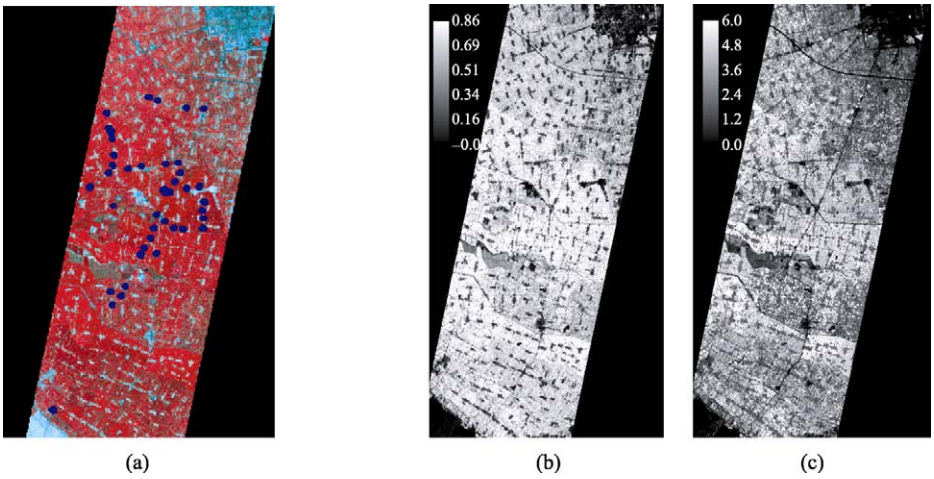

Fig. 2 LAI inversed from Hyperion data
(a) Hyperion image (locations of ground sample points); (b) NDVI; (c) LAI

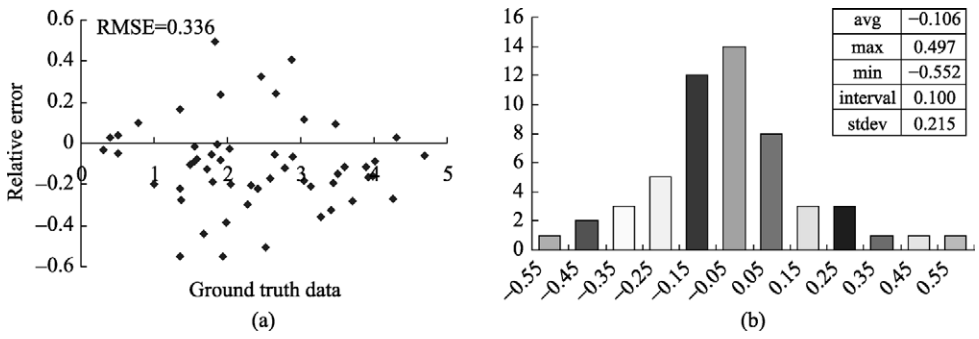

Fig. 3 Error Analysis of LAI inversion
(a) Scatter diagram of relative error; (b) Histogram of relative error

all the data will be used for discussing the scale effect in the LAI inversion.

4.1 The simplified equation for analysis of scale effect

The canopy reflectance model can be simply expressed as:

$$\begin{aligned}\rho &= F(\phi, \mathrm{LAI}, \mathrm{LAD}, N, C_{\mathrm{ab}}, C_{\mathrm{w}}, C_{\mathrm{other}}, \rho_{\mathrm{s}}) \\ &= f(\mathrm{LAI})\end{aligned} \tag{1}$$

where ρ is the canopy reflectance; ϕ are the external parameters of model; LAD is the average leaf angle; N is the number of layers; C_{ab} is the chlorophyll content; C_{w} is the leaf water content; C_{other} is the dry matter content; ρ_{s} is soil reflectance.

As known that there is nonlinear function relationship between LAI and NDVI (Zhao, 2003), then we use Eq. (1) to establish the relational between NDVI and LAI:

$$\mathrm{NDVI} = \frac{\rho_{\mathrm{nir}} - \rho_{\mathrm{r}}}{\rho_{\mathrm{nir}} + \rho_{\mathrm{r}}} = \frac{f_1(\mathrm{LAI}) - f_2(\mathrm{LAI})}{f_1(\mathrm{LAI}) + f_2(\mathrm{LAI})} = G(\mathrm{LAI})$$

that is,

$$\mathrm{LAI} = g(\mathrm{NDVI}) \tag{2}$$

Eq. (2) is used as a basis for the scale effect analysis and bias correction later. The formula is very simple, and the NDVI is sensitive to the land cover and can reflect the background impact of plant canopy, so it is conducive to analyze the scale effect of multi-scales LAI inversion under variable spatial structures.

4.2 Scale effect of LAI inversion

The low resolution LAI are achieved in two ways. '$\mathrm{LAI_{mean}}$', the mean of LAI (30m) , is directly calculated from Hyperion and used as the low resolution LAI true value (Fig. 4(a)). '$\mathrm{LAI_p}$', the LAI retrieval from linear aggregation image (300m) of Hyperion 30m reflectance data, is used as the low resolution LAI inversion value (Fig. 4(b)).

$\mathrm{LAI_p}$ retrieved from low resolution remote sensing image is an underestimation compared with $\mathrm{LAI_{mean}}$ (Table 2), which may caused by the model non-linearity and landscape spatial heterogeneity.

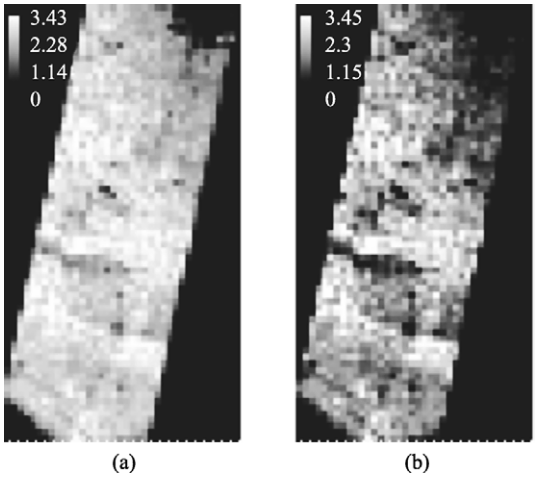

Fig. 4 Results of two up-scaling methods
(a) $\mathrm{LAI_{mean}}$; (b) $\mathrm{LAI_p}$

Table 2 Comparison of LAI before and after correction

	min	max	mean
$\mathrm{LAI_p}$	0	3.45	1.27
$\mathrm{LAI_r}$	0	3.39	1.96
$\mathrm{LAI_{mean}}$	0	3.43	2.06

$\mathrm{err}=\mathrm{LAI_p}-\mathrm{LAI_{mean}}$ is defined as the error factor of up-scale LAI inversion and the following formulas are obtained based on Eq. (3): $\mathrm{LAI_p} = g(\mathrm{NDVI_p}) \approx g\left(\frac{1}{n}\sum_{i=1}^{n}\mathrm{NDVI}_i\right)$. Therefore,

$$\begin{aligned}\mathrm{err} &= \mathrm{LAI_p} - \mathrm{LAI_{mean}} = g\left(\frac{1}{n}\sum_{i=1}^{n}\mathrm{NDVI}_i\right) - \frac{1}{n}\sum_{i=1}^{n} g(\mathrm{NDVI}_i) \\ &= g(m\mathrm{NDVI}) - \frac{1}{n}\sum_{i=1}^{n} g(\mathrm{NDVI}_i)\end{aligned} \tag{3}$$

In Eq.(3), $m\mathrm{NDVI} = \frac{1}{n}\sum_{i=1}^{n}\mathrm{NDVI}_i$, where '$m$NDVI' is the aggregated NDVI value within the large scale NDVI, $\mathrm{NDVI_{min}}$, $\mathrm{NDVI_{max}}$ are the minimum and maximum of the small scale NDVI values, and $m\mathrm{NDVI} \in [\mathrm{NDVI_{min}}, \mathrm{NDVI_{max}}]$. Then the Taylor Mean Value Theorem is applied to design the polynomial expansion of '$\mathrm{LAI_{mean}}$' around mNDVI.

$$\begin{aligned}\mathrm{LAI_{mean}} = \frac{1}{n}\Bigg\{\sum_{i=1}^{n}[&g(m\mathrm{NDVI}) + g'(m\mathrm{NDVI})(\mathrm{NDVI}_i - m\mathrm{NDVI}) \\ &+ \frac{g''(m\mathrm{NDVI})(\mathrm{NDVI}_i - m\mathrm{NDVI})^2}{2}] + R\Bigg\}\end{aligned}$$

where R is a higher order infinitesimal of $(\mathrm{NDVI}_i - m\mathrm{NDVI})^2$, therefore,

$$\begin{aligned}\mathrm{err} &\approx g(m\mathrm{NDVI}) - g(m\mathrm{NDVI}) \\ &\quad - \frac{1}{n}\sum_{i=1}^{n} g'(m\mathrm{NDVI})(\mathrm{NDVI}_i - m\mathrm{NDVI}) \\ &\quad - \frac{1}{2n}\sum_{i=1}^{n} g''(m\mathrm{NDVI})(\mathrm{NDVI}_i - m\mathrm{NDVI})^2 \\ &= -g'(m\mathrm{NDVI})\left(\frac{1}{n}\sum_{i=1}^{n}(\mathrm{NDVI}_i - m\mathrm{NDVI})\right) \\ &\quad - \frac{1}{2}g''(m\mathrm{NDVI})\left(\frac{1}{n}\sum_{i=1}^{n}(\mathrm{NDVI}_i - m\mathrm{NDVI})^2\right) \\ &= -\frac{1}{2}g''(m\mathrm{NDVI})\left(\frac{1}{n}\sum_{i=1}^{n}(\mathrm{NDVI}_i - m\mathrm{NDVI})^2\right)\end{aligned} \tag{4}$$

where $\frac{1}{n}\sum_{i=1}^{n}(\mathrm{NDVI}_i - m\mathrm{NDVI})^2$ is the variance of NDVI value at the small scale image, and $\sigma_{\mathrm{NDVI}} = \frac{1}{n}\sum_{i=1}^{n}(\mathrm{NDVI}_i - m\mathrm{NDVI})^2$. Finally, the error factor is simplified by Eq. (5):

$$\mathrm{err} = \mathrm{LAI_p} - \mathrm{LAI_{mean}} = -\frac{1}{2}\sigma_{\mathrm{NDVI}} \times g''(m\mathrm{NDVI}) \tag{5}$$

Therefore, the errors of LAI retrieved from large scale image can be adjusted through variance of NDVI value before agg-

regated and the second order differential equation of g. That is, scale conversion of LAI can be achieved by Eq. (5).

5 ERROR CORRECTION AND ANALYSIS

5.1 Error correction

LAI retrieved from low resolution remote sensing image is thus adjusted by Eq. (5):

$$\mathrm{LAI_r} = \mathrm{LAI_p} - \mathrm{err} = \mathrm{LAI_p} + \frac{1}{2}\sigma_{\mathrm{NDVI}} \times g''(m\mathrm{NDVI}) \quad (6)$$

Where $\mathrm{LAI_r}$ is the low resolution LAI that has been corrected, $g''(m\mathrm{NDVI})$ is the second order differential equation of g. Based on the ground truth data, the regression function of LAI and NDVI is established as follow:

$$\mathrm{LAI} = g(\mathrm{NDVI}) = 11.602\mathrm{NDVI}^3 - 6.793\mathrm{NDVI}^2 + 4.306\mathrm{NDVI} + 0.002 \quad (7)$$
$$R^2 = 0.81$$

In the Eq. (7), NDVI is calculated from Hyperion band 34, 50, and the second order differential equation of g is $g''(m\mathrm{NDVI}) = 69.612\, m\mathrm{NDVI} - 13.586$, so,

$$\mathrm{LAI_r} = \mathrm{LAI_p} + \sigma_{\mathrm{NDVI}}(34.806 m\mathrm{NDVI} - 6.793) \quad (8)$$

$\mathrm{LAI_r}$ is the result of correction by using Eq. (8). From the statistics in Table 2, it can be concluded that LAI values are closer to the "true value" after correction.

Before correction, LAI values are distributed in the upper left of the scatter (Fig. 5), indicating the underestimation of LAI retrieved from aggregated reflectance data. After correction, the correlation coefficient of $\mathrm{LAI_r}$ and $\mathrm{LAI_{mean}}$ is significantly increased to 0.85 and the averages of the two values are closer. It can be concluded that the method is effective because it takes the effects of spatial heterogeneity (variance) into account. Therefore, LAI of 30m resolution can be conversed to large scale through the method and the method can also be applied for the calibration of low resolution LAI products, such as MODIS LAI product.

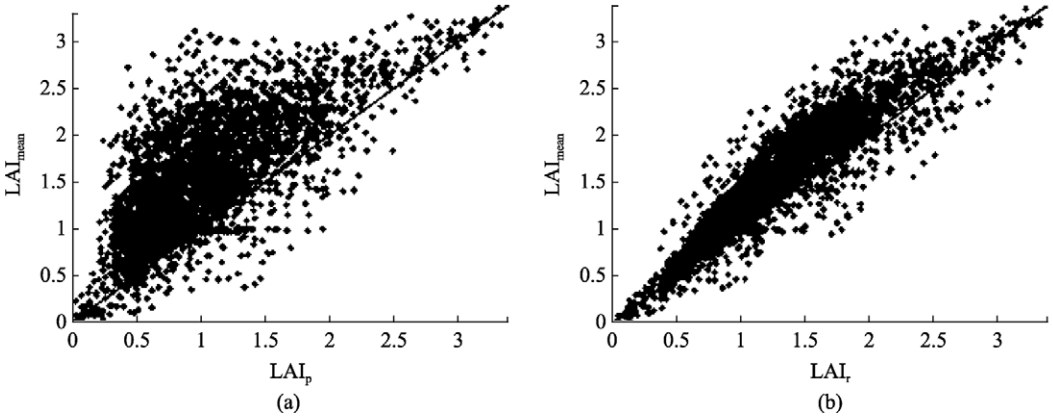

Fig. 5 Correlation between LAI and $\mathrm{LAI_{mean}}$ before and after correction

(a) Before correction; (b) After correction

5.2 Error analysis

Above analysis shows scale effect of LAI inversion from different resolution remote sensing images and underestimation of the inversion result from low resolution image. The influence factors are discussed in the following study.

5.2.1 The error caused by spatial heterogeneity

Due to the uneven distribution of vegetation, pixels consist of different land types appear during spectra linear aggregation. There will be a considerable uncertainty of the results if the ACRM model is applied to retrieving LAI in this region.

Base on Hyperion NDVI, formula f=(NDVI–$\mathrm{NDVI_s}$)/($\mathrm{NDVI_v}$–$\mathrm{NDVI_s}$) (where, NDVI is Normalized Difference Vegetation Index; $\mathrm{NDVI_s}$ is the NDVI of bare soil are; $\mathrm{NDVI_v}$ is the pure vegetation cover area) is applied to calculate vegetation coverage (Zhang, 1996), and then an inversion error is defined as the difference between $\mathrm{LAI_p}$ and $\mathrm{LAI_{mean}}$. Fig. 6 shows the relationship between errors and vegetation coverage, that the spatial distribution of vegetation will cause the scale errors. LAI inversion errors gradually increase with changes of vegetation coverage, reaching to the maximum at the coverage of 50%, while the NDVI variance of mixed pixel is also the greatest with the greatest spatial heterogeneity. When vegetation coverage is about 45%—55%, the relationship between inversion errors and vegetation cover is uncertainty. This is because when the vegetation coverage is determinate: (1) the vegetation spatial distributions within mixed pixel are inconsistent and effects of the interaction between sub-pixels are varying; (2) combinations of vegetation types within mixed pixel are not always the same. When vegetation coverage is high, pixel is of a better uniformity and the scale error is smaller. Because NDVI is sensitive to the vegetation cover and can reflect the background impact of plant canopy, we establish a scatter gram (Fig. 7) between NDVI variances and scale errors

to analyze the variation of errors. Fig. 7 shows that, at the low vegetation coverage, with the increase of spatial heterogeneity at the mixed pixel, the scale error of LAI inversion is also increased.

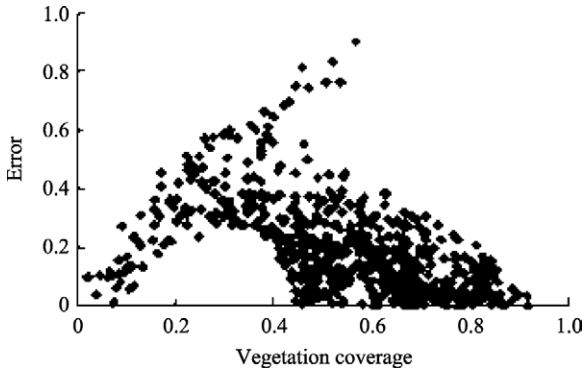

Fig. 6 Errors caused by spatial heterogeneity

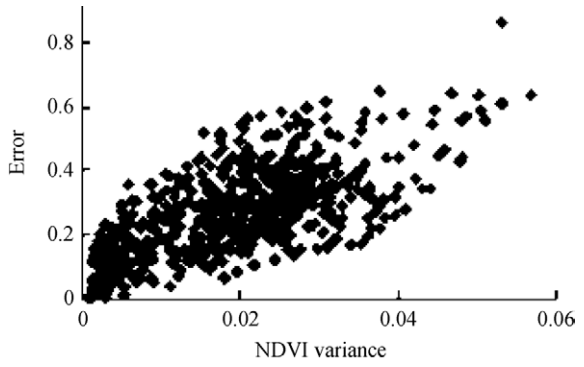

Fig. 7 Relationship between errors and NDVI variance

5.2.2 Error caused by model non-linearity

The model non-linearity is one of the reasons that caused the inversion error. By selecting an area consisted of bare soil and crops within the study area, we extract pure vegetation canopy reflectance within the mixed pixels. The effect of spatial heterogeneity is supposed to be eliminated. Then the true LAI (Xu, 2009) that consistent with the concept of crop sowing is calculated by applying the formula $\mathrm{LAI}_{\mathrm{mean}}' = \dfrac{\frac{1}{n}\sum_{i=1}^{n} f(\rho_i)}{a}$. Where $\mathrm{LAI}_{\mathrm{mean}}'$ does not mean the same as $\mathrm{LAI}_{\mathrm{mean}}$, $\mathrm{LAI}_{\mathrm{mean}}'$ ignore the spatial heterogeneity of the surface structure and can be applied to study the errors caused by model non-linearity.

$$\mathrm{err}' = f_{\mathrm{ACRM}}\left(\frac{\frac{1}{n}\sum_{i=1}^{n}\rho_i}{a}\right) - \frac{\frac{1}{n}\sum_{i=1}^{n} f_{\mathrm{ACRM}}(\rho_i)}{a} \qquad (9)$$

where ρ_i is the reflectance before aggregation, a is the proportion of crops.

Overall, error caused by model non-linearity is small (Fig. 8). The maximal error is about 0.12 when vegetation coverage is 50%. The conclusion is consistent with the studies of Zhang *et al.* (2008) and Chen *et al.* (2006). The model non-linearity does affect LAI inversion, but not the key factor, and can be ignored if the coverage is very low or coverage is much too high.

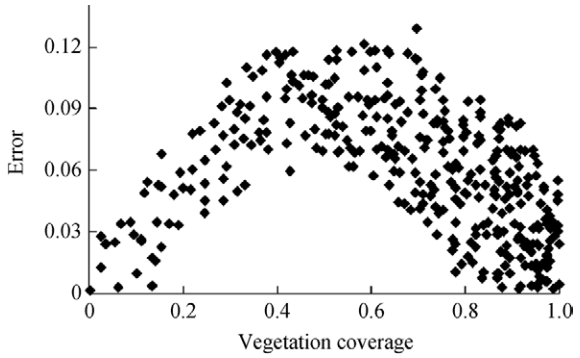

Fig. 8 Errors caused by model non-linearity

6 CONCLUSIONS

(1) ACRM model is introduced to retrieve crop LAI in the Yingke oasis of Heihe Basin. The LAI retrieved from low resolution data is underestimated. The average LAI directly calculated from Hyperion is about 2.06, but it is only 1.27 when the LAI is retrieved from up-scaling data. On the basis of LAI-NDVI regression equation, the Taylor Mean Value Theorem is applied to analysis error factors and achieve the correction of low resolution LAI values. The method could also be used for calibration of other low resolution LAI products, such as MODIS LAI product.

(2) After impact analysis of model non-linearity and landscape spatial heterogeneity on LAI inversion, it is found that the model non-linearity is one of the reasons that cause the inversion errors, but not the key factor, and can be ignored in some specific applications if the coverage is very low or coverage is much too high. The main factor that causes the scaling errors is the uneven distribution of surface vegetation, that is, the spatial heterogeneity is a key factor in LAI inversion. Although the scale bias is a coupling error caused by spatial heterogeneity and model non-linearity, it is not considered yet in this paper and need to be analyzed in further study.

(3) Further research will focus on ① studying the influence of the spatial heterogeneity caused by different combinations of vegetation (corn, wheat, and other vegetation), ② establishing an error correction model in multi-spectral reflectance space.

REFERENCES

Chen J, Ni S and Li J. 2006. Scaling effect and spatial variability in retrieval of vegetation LAI from remotely sensed data. *Acta Ecologica Sinica*, **26**(5): 1503—1508

Feng X M and Zhao Y S. 2005. A spectral-directional reflectance remote sensing model of the semiarid landscape. *Jounal of Remote Sensing*, **9**(4): 337—342

Garrigues S, Allard B D and Baret F. 2006. Influence of landscape

spatial heterogeneity on the non-linear estimation of leaf area index from moderate spatial resolution remote sensing date. *Remote Sensing of Environment*, **105**: 286—298

Jacquemoud S and Baret F. 1990. PROSPECT: A model of leaf optical properties spectra. *Remote Sensing of Environment*, **34**:75—91

Kuusk A. 1985. The hot spot effect of a uniform vegetative cover. *Soviet Journal of Remote Sensing*, **3**(4): 645—658

Kuusk A 2001. A two-layer canopy reflectance model. *Journal of Quantitative Spectroscopy & Radiative Transfer*, **71**: 1—9

Luo Y and Su N. 2002. Selection of optimal bands from remote sensing image based on information content. *Urban Geotechnical Investigation & Surveying*. **4**(4): 28—32

Tian Y H, Woodcock C E and Wang Y J. 2002. Multi-scale analysis and validation of the MODIS LAI product, I. Uncertainty assessment. *Remote Sensing of Environment*, **83**:414—430

Tian Y H and Wang Y J. 2003. Radiative transfer based scaling of LAI retrievals from reflectance data of different resolutions. *Remote Sensing of Environment*, **84**: 143—159

Verhoef W. 1984. Light scattering by leaf layers with application to canopy reflectance modeling: the SAIL model. *Remote Sensing of Environment*, **16**: 125—141

Xu Q Z, Zhang W C, Liu S C, Zhao D Z and Jiang J J. 2003. Retrieval of leaf area index for the Heihe River watershed by using remote sensing data. *Arid Zone Research*. **20**(4): 281—285

Xu X R. 2005. Remote Sensing Physics. Beijing: Peking University Press

Xu X R, Fan W J and Tao X. 2009. The spatial scaling effect of continuous canopy Leaves Area Index retrieved by remote sensing, *Science in China*, **52**(3): 393—401

Yao Y J, Liu Q, Liu Q H and Li X W. 2007. LAI inversion uncertainties in heterogeneous surface. *Journal of Remote Sensing*. **11**(6): 763—770

Zhang R H. 1996. Experimental Remote Sensing Model and Ground Basis. Beijing: Science Press

Zhang W C, Zhong S and Hu S Y. 2008. Spatial scale transferring study on Leaf Area Index derived from remotely sensed data in the Heihe River Basin, China. *Acta Ecologica Sinica*, **28**(6): 2495—2503

Zhao Y S. 2003. Theory and Method of Remote Sensing Application and Analysis. Beijing: Science Press

作物 LAI 的遥感尺度效应与误差分析

朱小华[1,2], 冯晓明[3], 赵英时[2], 宋小宁[2]

1. 中国科学院遥感应用研究所, 北京 100101;
2. 中国科学院研究生院, 北京 100049;
3. 中国科学院生态环境研究中心, 北京 100085

摘 要: 以黑河中游盈科绿洲为研究区, 利用 Hyperion 高光谱数据, 采用双层冠层反射率模型(ACRM)迭代运算反演 LAI; 通过 LAI 的均值化(LAI_{mean})以及 Hyperion 数据反射率线性累加反演 LAI(LAI_p), 定量分析 LAI 反演的尺度效应; 从模型的非线性和地表景观结构的空间异质性 2 个方面分析引起反演误差的原因, 并在 LAI-NDVI 回归方程的基础上利用泰勒展开的方法对低分辨率数据反演结果进行了误差纠正。结果表明, 地表景观结构的空间异质性是造成多尺度 LAI 反演误差的关键因素, 通过泰勒展开式能很好地实现大尺度数据 LAI 反演结果的误差纠正。

关键词: Hyperion, 叶面积指数, 尺度效应, 反演, 误差纠正

中图分类号: TP751.1 文献标识码: A

引用格式: 朱小华, 冯晓明, 赵英时, 宋小宁. 2010. 作物 LAI 的遥感尺度效应与误差分析. 遥感学报, **14**(3): 579—592
Zhu X H, Feng X M, Zhao Y S and Song X N. 2010. Scale effect and error analysis of crop LAI inversion. *Journal of Remote Sensing*. **14**(3): 579—592

1 引 言

叶面积指数(leaf area index, LAI)是表征作物生长状况的重要物理参数, 近年来通过遥感技术反演 LAI 的尺度效应问题日益受到重视。Tian 等(2002, 2003)曾分别对 MODIS 的 LAI 产品进行了多尺度分析和验证, 并进行了采样方案的设计, 他们指出, 随着尺度的增加, 当一个植被类型中混入大量其他植被类型时, 会产生较大的反演误差。Garrigues 等(2006)利用 NDVI, R, NIR 建立了基于单变量和双变量的半经验模型, 分析了 LAI 反演的尺度效应问题并进行了多分辨率反演结果的误差纠正研究。姚延娟等(2007)对异质性地表的 LAI 反演进行了不确定性分析指出, 不同组分形成的混合像元对 LAI 的反演结果影响很大。张万昌等(2008)利用 ETM 数据对不同分辨率反演 LAI 中的尺度效应问题进行了定量分析, 提出了一种基于 NDVI 像元分解的升尺度转换方法。徐希孺等(2009)在作物冠层反射率模型的基础上, 讨论了 LAI 尺度效应的产生机制, 利用数值模拟方法建立了不同尺度之间的 LAI 转换公式。这些文献指出地表植被分布的不均一带来尺度效应, 即不同分辨率的遥感影像反演 LAI 存在一定的差异。

本文以黑河中游盈科地区为研究区, 利用 Hyperion 高光谱数据, 采用双层冠层反射率模型反演 LAI; 通过 Hyperion 数据反射率线性累加来获取不同分辨率的遥感影像, 研究分析 LAI 反演的尺度效应问题, 并在 LAI-NDVI 回归方程的基础上利用泰勒展开的方法对低分辨率数据反演结果进行了误差纠正, 实现了大尺度 LAI 的校正。

2 研究区与数据

2.1 研究区概况

黑河流域发源于青海省祁连县, 位于祁连山和河西走廊的中段, 北部与内蒙古自治区接壤, 东部与武威盆地相连, 西部与疏勒流域毗邻, 是中国西

收稿日期: 2009-07-13; 修订日期: 2009-10-26
基金项目: 国家重点基础研究发展计划“973”项目(编号: 2007CB714407)和国家自然科学基金项目(编号: 40801070)。
第一作者简介: 朱小华(1986—), 女, 博士研究生, 2007 年毕业于中国农业大学信息管理系, 主要从事定量遥感应用研究。Zhuxh0118@163.com。
通讯作者: 冯晓明, E-mail: fengxm@rcees.ac.cn。

北地区第二大内陆河流域，流域面积约 142900km^2。受中高纬度的西风带环流控制和极地冷气团影响，年平均降雨量稀少，加上人类活动的影响，黑河流域植被覆盖不均一、季节变化大。本研究区集中于黑河中游盈科绿洲区，主要植被类型为小麦、玉米等(图 1)。

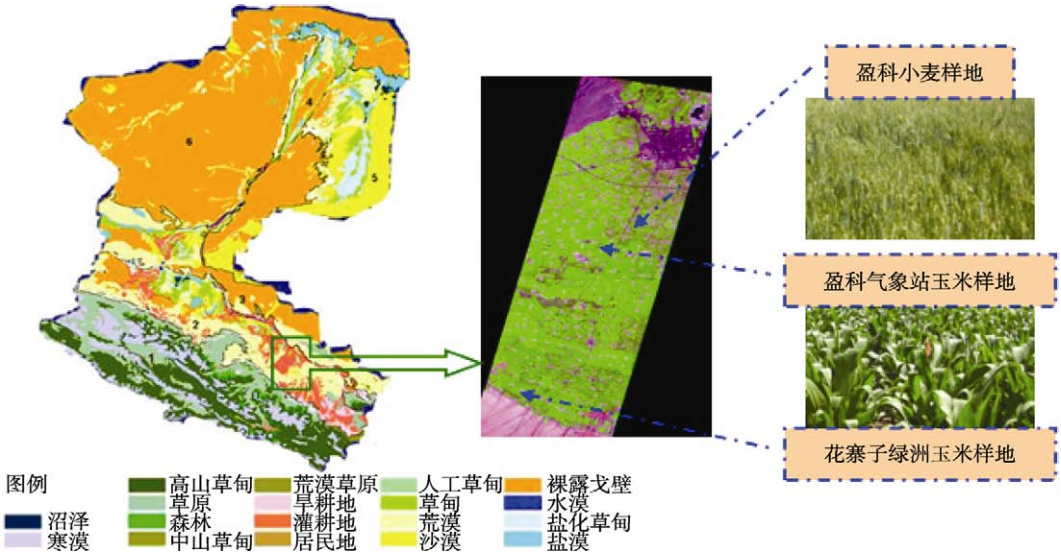

图 1　研究区示意图

2.2　数据预处理

2.2.1　数据介绍

研究区的遥感数据为黑河盈科绿洲 2008-07-15 的 Hyperion 高光谱数据。Hyperion 是美国 NASA 于 2000-11-21 发射升空的 EO-1 地球观测卫星上搭载的 3 种传感器之一，是以推扫方式获取可见光-近红外和短波红外光谱数据，共 242 个波长、空间分辨率 30m。相应的地面数据为 2008 年 6 月 13—26 日盈科绿洲样地的实测数据，由于玉米等处于成熟期，叶面积指数相对稳定，波动范围可以接受。地面实测 LAI 数据主要通过 LAI- 2000、LAI-3000 仪器和人工测定两种方式同时获取，即采用人工直接测量样本叶片长度和宽度，结合仪器测量 LAI 结果求算各类作物的叶面积指数校正系数，利用各校正系数乘以相应作物的叶长宽，得到各类作物的叶面积指数。

2.2.2　数据预处理

采用 ENVI 中的大气校正模块 FLAASH 对 Hyperion 数据进行大气校正，将表观反射率转换为地表地物反射率。利用同区域已经做过几何精纠正的 ETM 数据，通过图像对图像的配准方法对 Hyperion 数据进行几何纠正，纠正时各控制点的 RMS 控制在 0.5 个像元以内, RMSerr 误差值为 0.28, 图像经几何纠正后的投影为 UTM 投影。

由于高光谱遥感数据波长间隔小，波段之间存在大量的信息冗余，本研究在分析了研究区特点后，按标准差尽可能大、相关性系数尽可能小的原则，对 Hyperion 波段数据进行了最佳波段选择(罗音等, 2002)。具体过程如下: (1)去掉标准差小，即信息量较少的波段; (2)把可见光(蓝、绿、红)、近红外、短波红外分为 5 组，每组按信息量排列选择 7 个标准差较大的波段; (3)各组依次进行相关性分析，每组选取两三个相互之间相关性较小的波段。最后选取 14 个波段(表 1)。

表 1　最佳波段选择结果

序号	Hyperion 原始波段	波长/nm
1	14	487.87
2	18	528.57
3	21	559.09
4	23	579.45
5	26	609.97
6	34	691.37
7	37	721.90
8	40	752.43
9	50	854.18
10	54	894.88
11	83	972.99
12	88	1023.40
13	92	1063.79
14	96	1104.18

3 LAI 模型反演

在农作物生长成熟期，成行播种的结构特征逐渐消失，农作物呈现近似水平均一的结构特征，如图 1。根据研究区农作物生长情况，选择了适合植被水平均一分布的反射率计算模型——双层冠层反射率模型 ACRM(Kuusk, 2001)。该模型嵌套了 PROSPECT 叶片光学模型(Jacquemoud & Baret, 1990)，通过叶片结构参数和叶片生化参数的函数关系，模拟了叶片从 400—2500nm 的反射率和透射率，并能够很好地解释叶片表面的镜面反射和叶片尺度上的“热点”现象，同时具有较高的计算效率。模型中的多次散射采用了与 SAIL 模型(Verhoef, 1984)相同的 4 流参数化计算方案。即假设植物冠层是由方位随机分布的水平、均一及无限扩展的各向同性叶片组成的混合体，叶片具有漫散射的反射和透射特性，在给定冠层结构参数和环境参数时，可以计算出任意太阳高度和观测方向的冠层反射率。Kuusk (1985)对 SAIL 模型进行了改进，考虑冠层的热点以及叶片镜面反射的影响。ACRM 模型基于辐射传输理论模拟双层结构冠层，不依赖于植被的具体类型或背景环境变化，具有较好的普适性(Verhoef, 1984; 冯晓明 & 赵英时, 2005)。

图 2(a)(b)为 2008-07-15 的黑河盈科绿洲区 Hyperion 图像与 NDVI 数据。在用 ACRM 模型进行 LAI 反演前，我们利用研究区地面实测数据对模型的输入参数(如叶面积指数，叶片大小参数，叶绿素含量、土壤参数等)进行了设置。图 2(c)为模型迭代反演的结果。利用黑河联合实验地面 LAI 实测数据对本次的反演结果进行验证(图 3)，从反演相对误差直方图分析可以看出，LAI 反演值与 LAI 实测值存在很好的一致性，两者的相关关系达 0.79，均方根误

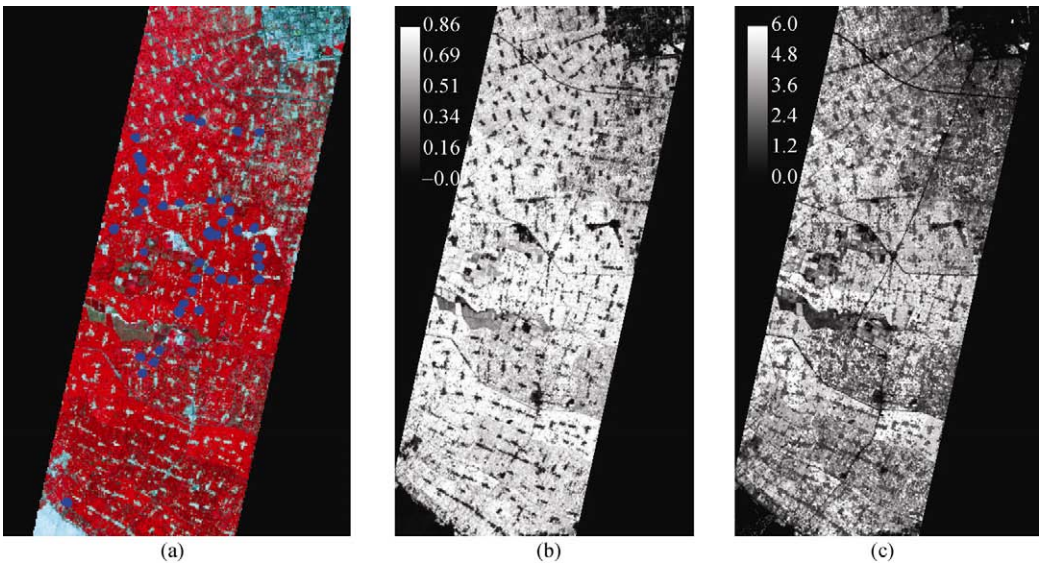

图 2 研究区 Hyperion 图像 LAI 反演

(a) 假彩色图像(标识有地面样点位置); (b) NDVI; (c) LAI

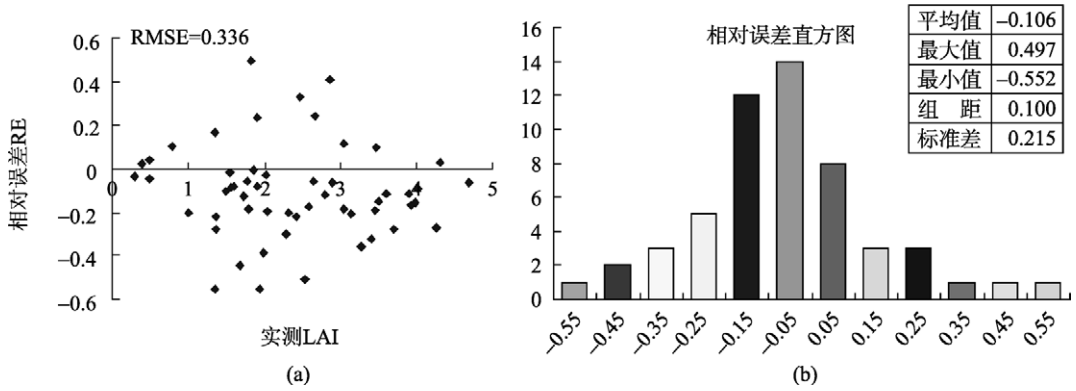

图 3 LAI 反演误差分析

(a) 反演相对误差散点图; (b) 反演相对误差直方图

差 RMSE 为 0.336。验证结果表明，基于 ACRM 模型反演的 LAI 较好地反映了地面状况，可以用于进一步的尺度效应分析。

4 尺度效应定量分析

ACRM 模型反演仅为了得到研究区的 LAI，本文的重点是采用 LAI-NDVI 之间的关系研究不同尺度下 LAI 反演的尺度效应，分析其来源以及进行误差纠正。为了使不同尺度数据反演叶面积指数不受传感器等外在因素影响，研究采用 Hyperion 30m 数据线性聚合获得多尺度的遥感图像，用于分析讨论不同分辨率遥感图像反演 LAI 的尺度效应问题。

4.1 尺度效应分析的简化方程

ACRM 冠层反射率模型可以简单表示为:

$$\rho = F(\phi, \mathrm{LAI}, \mathrm{LAD}, N, C_{\mathrm{ab}}, C_{\mathrm{w}}, C_{\mathrm{other}}, \rho_{\mathrm{s}}) = f(\mathrm{LAI}) \quad (1)$$

式中，ρ为冠层的反射率；ϕ为模型外部参数；LAI 为叶面积指数，LAD 为平均叶倾角；N 为叶片层数，C_{ab} 为叶绿素含量，C_{w} 为叶片含水量，C_{other} 为干物质等含量；ρ_{s} 为土壤反射率。

已知 LAI 与 NDVI 之间存在非线性函数关系(赵英时，2003)，利用式(1)建立 NDVI 与 LAI 之间的函数关系式:

$$\mathrm{NDVI} = \frac{\rho_{\mathrm{nir}} - \rho_{\mathrm{r}}}{\rho_{\mathrm{nir}} + \rho_{\mathrm{r}}} = \frac{f_1(\mathrm{LAI}) - f_2(\mathrm{LAI})}{f_1(\mathrm{LAI}) + f_2(\mathrm{LAI})} = G(\mathrm{LAI})$$

即，

$$\mathrm{LAI} = g(\mathrm{NDVI}) \quad (2)$$

从 ACRM 模型出发简化获得 LAI 与 NDVI 之间的回归关系方程式(2)，该公式在本次研究中并不用于 LAI 反演，仅作为后期空间结构变化 LAI 尺度效应分析和偏差纠正的基础。该公式简单，NDVI 对植被覆盖敏感，能反映出植物冠层的背景影响，有利于分析空间结构变化下多尺度 LAI 反演的尺度效应问题。

4.2 LAI 反演的尺度效应

采用两种方法从 Hyperion 数据反演 LAI(30m)尺度上推到 300m: 一是将由 Hyperion 数据反演所得的 LAI(30m)直接均值化得到 $\mathrm{LAI}_{\mathrm{mean}}$(300m)，用以模拟低分辨率 LAI 信息(本文中暂定为低分辨率 LAI 真实值，图 4(a))；二是将原 Hyperion 数据(30m)线性聚合为低分辨率的图像数据(300m)，经模型反演得到 $\mathrm{LAI}_{\mathrm{p}}$(本文中暂定为低分辨率 LAI 反演值，图 4(b))。

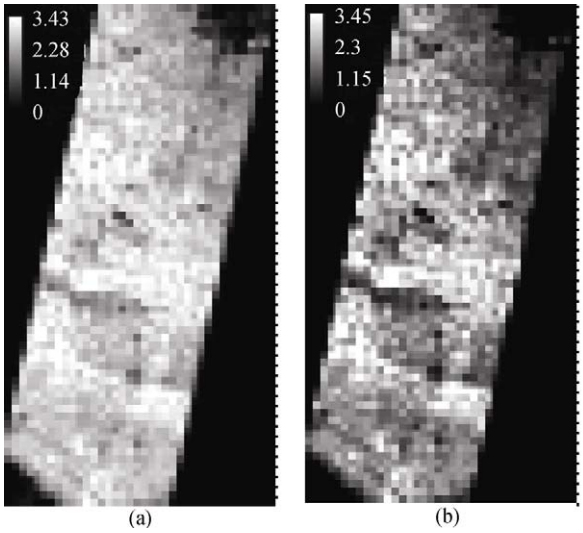

图 4 Hyperion--LAI 两种尺度变换方法的结果图
(a) $\mathrm{LAI}_{\mathrm{mean}}$; (b) $\mathrm{LAI}_{\mathrm{p}}$

低分辨率影像遥感反演结果 $\mathrm{LAI}_{\mathrm{p}}$ 与 $\mathrm{LAI}_{\mathrm{mean}}$ 存在一定程度的误差。由表 2 分析可知，经过线性聚合后再经模型反演得到的 LAI 值存在一定程度的低估现象，即 ACRM 模型的非线性和研究区景观的空间异质性造成 LAI 反演的尺度效应。

表 2 误差纠正前后 **LAI** 值统计信息比较

	min	max	mean
$\mathrm{LAI}_{\mathrm{p}}$	0	3.45	1.27
$\mathrm{LAI}_{\mathrm{r}}$	0	3.39	1.96
$\mathrm{LAI}_{\mathrm{mean}}$	0	3.43	2.06

定义 $\mathrm{err}=\mathrm{LAI}_{\mathrm{p}}-\mathrm{LAI}_{\mathrm{mean}}$ 为升尺度后遥感影像反演 LAI 的误差因子。由式(2)可知，$\mathrm{LAI}_{\mathrm{mean}} = \frac{1}{n}\sum_{i=1}^{n}\mathrm{LAI}_i = \frac{1}{n}\sum_{i=1}^{n} g(\mathrm{NDVI}_i)$；可得，$\mathrm{LAI}_{\mathrm{p}} = g(\mathrm{NDVI}_{\mathrm{p}}) \approx g\left(\frac{1}{n}\sum_{i=1}^{n}\mathrm{NDVI}_i\right)$。

$$\begin{aligned}\mathrm{err} &= \mathrm{LAI}_{\mathrm{p}} - \mathrm{LAI}_{\mathrm{mean}} \\ &= g\left(\frac{1}{n}\sum_{i=1}^{n}\mathrm{NDVI}_i\right) - \frac{1}{n}\sum_{i=1}^{n} g(\mathrm{NDVI}_i) \\ &= g(m\mathrm{NDVI}) - \frac{1}{n}\sum_{i=1}^{n} g(\mathrm{NDVI}_i)\end{aligned} \quad (3)$$

其中，$m\mathrm{NDVI} = \frac{1}{n}\sum_{i=1}^{n}\mathrm{NDVI}_i$，为与大尺度图像像元对应的 n 个小尺度图像像元 NDVI 的均值，若 $\mathrm{NDVI}_{\mathrm{min}}$，$\mathrm{NDVI}_{\mathrm{max}}$ 为 n 个小尺度图像像元 NDVI 里的最小和最大值，则 $m\mathrm{NDVI}\in[\mathrm{NDVI}_{\mathrm{min}}, \mathrm{NDVI}_{\mathrm{max}}]$。利用泰勒(Taylor)中值定理对函数 $\mathrm{LAI}_{\mathrm{mean}} = \frac{1}{n}\sum_{i=1}^{n} g(\mathrm{NDVI}_i)$按($\mathrm{NDVI}_i$=$m$NDVI)进行多项式展开:

$$\mathrm{LAI}_{\mathrm{mean}}=\frac{1}{n}\left\{\sum_{i=1}^{n}[g(m\mathrm{NDVI})+g'(m\mathrm{NDVI})(\mathrm{NDVI}_i-m\mathrm{NDVI})+\frac{g''(m\mathrm{NDVI})(\mathrm{NDVI}_i-m\mathrm{NDVI})^2}{2}]+R\right\}$$

这里的 R 为比$(\mathrm{NDVI}_i-m\mathrm{NDVI})^2$高阶的无穷小值，故，

$$\begin{aligned}\mathrm{err}&\approx g(m\mathrm{NDVI})-g(m\mathrm{NDVI})\\&\quad-\frac{1}{n}\sum_{i=1}^{n}g'(m\mathrm{NDVI})(\mathrm{NDVI}_i-m\mathrm{NDVI})\\&\quad-\frac{1}{2n}\sum_{i=1}^{n}g''(m\mathrm{NDVI})(\mathrm{NDVI}_i-m\mathrm{NDVI})^2\\&=-g'(m\mathrm{NDVI})\left(\frac{1}{n}\sum_{i=1}^{n}(\mathrm{NDVI}_i-m\mathrm{NDVI})\right)\\&\quad-\frac{1}{2}g''(m\mathrm{NDVI})\left(\frac{1}{n}\sum_{i=1}^{n}(\mathrm{NDVI}_i-m\mathrm{NDVI})^2\right)\\&=-\frac{1}{2}g''(m\mathrm{NDVI})\left(\frac{1}{n}\sum_{i=1}^{n}(\mathrm{NDVI}_i-m\mathrm{NDVI})^2\right)\end{aligned}\quad(4)$$

其中，$\frac{1}{n}\sum_{i=1}^{n}(\mathrm{NDVI}_i-m\mathrm{NDVI})^2$ 为小尺度图像 n 个像元NDVI的方差，令$\sigma_{\mathrm{NDVI}}=\frac{1}{n}\sum_{i=1}^{n}(\mathrm{NDVI}_i-m\mathrm{NDVI})^2$。最后，

$$\begin{aligned}\mathrm{err}&=\mathrm{LAI}_{\mathrm{p}}-\mathrm{LAI}_{\mathrm{mean}}\\&=-\frac{1}{2}\sigma_{\mathrm{NDVI}}\times g''(m\mathrm{NDVI})\end{aligned}\quad(5)$$

可见，大尺度数据反演 LAI 的误差可以通过聚合前图像NDVI的方差和相关函数 g 的二阶微分方程来进行调整。也就是说，可通过式(5)进行尺度转换。

5 误差纠正与分析

5.1 误差纠正

利用公式(5)对低分辨率遥感图像的反演结果进行误差调整，

$$\begin{aligned}\mathrm{LAI}_{\mathrm{r}}&=\mathrm{LAI}_{\mathrm{p}}-\mathrm{err}\\&=\mathrm{LAI}_{\mathrm{p}}+\frac{1}{2}\sigma_{\mathrm{NDVI}}\times g''(m\mathrm{NDVI})\end{aligned}\quad(6)$$

$\mathrm{LAI}_{\mathrm{r}}$ 是误差纠正后的低分辨率叶面积指数，$g''(m\mathrm{NDVI})$为方程 LAI=g(NDVI)的二阶微分，利用地面实测数据建立 LAI 与 NDVI 之间的回归关系:

$$\begin{aligned}\mathrm{LAI}&=g(\mathrm{NDVI})\\&=11.602\mathrm{NDVI}^3-6.793\mathrm{NDVI}^2\\&\quad+4.306\mathrm{NDVI}+0.002\\R^2&=0.81\end{aligned}\quad(7)$$

其中，NDVI 采用 Hyperion 第 34、50 波段计算获得。由式(7) LAI=g(NDVI)可得，

$$\begin{aligned}&g''(m\mathrm{NDVI})=69.612m\mathrm{NDVI}-13.586,\\&\mathrm{LAI}_{\mathrm{r}}=\mathrm{LAI}_{\mathrm{p}}+\sigma_{\mathrm{NDVI}}(34.806m\mathrm{NDVI}-6.793)\end{aligned}\quad(8)$$

利用式(8)可调整大尺度 LAI 反演结果。表 2 为 $\mathrm{LAI}_{\mathrm{r}}$, $\mathrm{LAI}_{\mathrm{p}}$, $\mathrm{LAI}_{\mathrm{mean}}$的统计信息比较。由表 2 可见，经式(8)调整后的 $\mathrm{LAI}_{\mathrm{r}}$更接近于“真值”$\mathrm{LAI}_{\mathrm{mean}}$。

从图 5 误差纠正前后 $\mathrm{LAI}_{\mathrm{p}}$, $\mathrm{LAI}_{\mathrm{r}}$与 $\mathrm{LAI}_{\mathrm{mean}}$之间的关于 $y=x$ 关系拟合结果分析中看出，纠正前 LAI 值偏离集中于上侧，说明聚合数据 LAI 反演结果存在一定程度的低估；纠正后，LAI 均值得到较好的提高且较接近 $\mathrm{LAI}_{\mathrm{mean}}$值，两者之间的相关关系也显著提高到 0.85，说明该方法考虑到了地表的空间异质

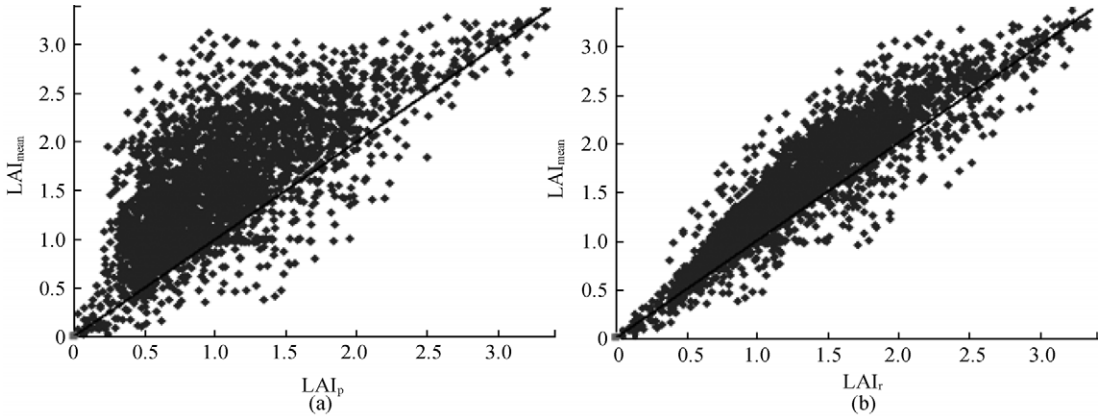

图 5 误差纠正前后 LAI 值与 $\mathrm{LAI}_{\mathrm{mean}}$的相关关系

(a) 误差纠正前; (b) 误差纠正后

性的影响(方差)，能较好地应用于低分辨率遥感数据 LAI 反演结果的纠正。通过该方法还可以将 30m 分辨率的 LAI 结果升尺度转换到其他分辨率结果，也可以用于 MODIS 等低分辨率 LAI 产品的校正。

5.2 误差分析

由表 2 可知，不同分辨率遥感影像 LAI 反演结果存在尺度效应，低分辨率 LAI 反演结果存在低估。景观的空间异质性和 ACRM 模型的非线性是 LAI 反演尺度效应的来源。

5.2.1 空间异质性结构引起的误差

利用光谱线性聚合获取大尺度影像，由于地表植被空间结构分布不均一，出现了植被与其他地类异质性组合的混合像元，应用基于像元下植被水平均一分布的反射率模型(ACRM)来计算 LAI 值，必然带来很大的不确定性。

基于 Hyperion NDVI，利用公式 $f=(\mathrm{NDVI}-\mathrm{NDVI_s})/(\mathrm{NDVI_v}-\mathrm{NDVI_s})$ (其中，NDVI 为植被归一化指数; $\mathrm{NDVI_s}$ 为裸土区的 NDVI 值; $\mathrm{NDVI_v}$ 纯植被覆盖区的 NDVI 值)计算研究区的植被覆盖度信息(张仁华, 1996)，然后采用 30m 的 Hyperion 数据线性聚合后经模型反演的结果 $\mathrm{LAI_p}$ 与 30m 的 LAI 信息直接均值化的结果 $\mathrm{LAI_{mean}}$ 差值得到低分辨率数据反演误差。从图 6 反演误差与植被覆盖度的变化关系看出，地表植被的空间分布会引起 LAI 反演的尺度误差。随着植被覆盖度的增加, LAI 反演的尺度误差逐渐增大，并在 0.5 附近达到最大，此时混合像元内的 NDVI 方差最大，即空间异质性最大。在植被覆盖度 45%—55%之间, LAI 反演的尺度误差与植被覆盖度之间的关系存在很大的不确定性。这是因为在植被覆盖比例相同的情况下，(1)植被在大尺度混合像元内的空间分布不一致，亚像元之间的相互作用影响的不一致性；(2)不同植被在大尺度混合像元内的组合不一致。在植被覆盖度较高区域，像元的均一性较好, LAI 反演的尺度误差偏小。由于 NDVI 对植被覆盖敏感，能反映出植物冠层的背景影响，通过建立混合像元内 NDVI 方差与尺度误差之间的散点图(图 7)发现，在植被覆盖度较低区域，随着 NDVI 方差的增加，即混合像元内异质性的增加，LAI 反演的尺度误差变大。说明地表空间异质性是大尺度影像 LAI 反演误差的主要来源，也是 LAI 尺度误差纠正的关键。

5.2.2 算法非线性引起的误差

算法的非线性是引起反演误差的原因之一，选取覆盖类型为裸土与农作物的混合区域作为研究区，

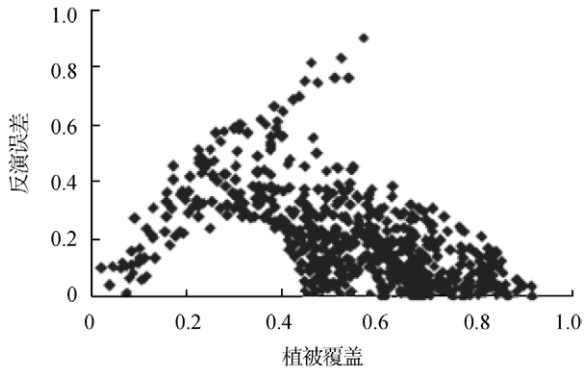

图 6 空间异质性造成的反演误差

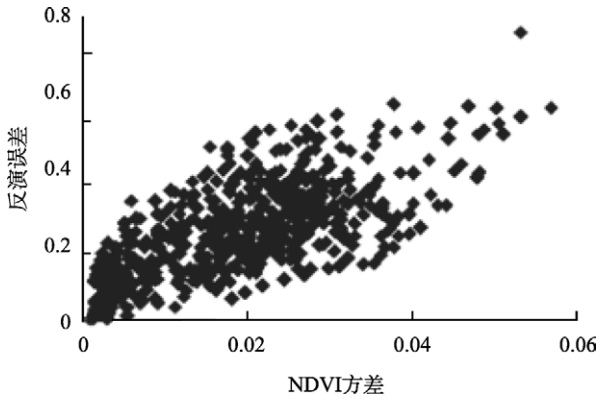

图 7 反演误差与 NDVI 像元方差之间的关系

从提取混合像元内部纯植被冠层反射率入手，理论上，该处理消除了空间异质性的影响。然后利用 $\mathrm{LAI_{mean}}'=\dfrac{\frac{1}{n}\sum_{i=1}^{n}f(\rho_i)}{a}$ 建立理论上符合作物播种概念的真实叶面积指数(徐希孺等，2009)，这里的 $\mathrm{LAI_{mean}}'$不同于前面的 $\mathrm{LAI_{mean}}$，没有考虑地表结构的空间异质性，可以应用于研究 ACRM 模型的非线性带来的误差。

$$\mathrm{err}'=f_{\mathrm{ACRM}}\left(\frac{\frac{1}{n}\sum_{i=1}^{n}\rho_i}{a}\right)-\frac{\frac{1}{n}\sum_{i=1}^{n}f_{\mathrm{ACRM}}(\rho_i)}{a} \qquad (9)$$

式中, ρ_i 为聚合前像元反射率, a 为农作物比例。

总体来说由 ACRM 模型的非线性算法引起的 LAI 反演误差较小(图 8)，在地面植被覆盖度达 50%时，误差最大，但是也仅为 0.12 左右，该结论与张万昌等(2008)、陈健等(2006)等的观点较为一致。模型的非线性也是引起不同分辨率反演结果误差的原因之一，但不是关键因素，在覆盖度很低或覆盖度较高的时候可以结合具体的应用予以忽略。

由此可知，相对于模型的非线性，地表景观结构的空间异质性是引起 LAI 反演结果误差的主要原因。

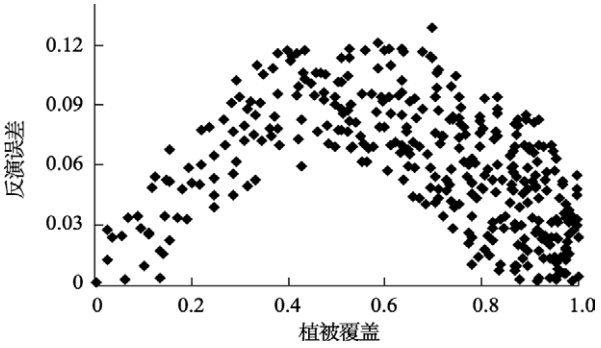

图 8 模型非线性引起的反演误差

6 结 论

(1) 本研究采用 ACRM 模型反演黑河盈科灌区的农作物 LAI, 采用 Hyperion 数据像元线性聚合获得多尺度的遥感图像, 发现低分辨率遥感图像在反演 LAI 时存在一定的低估现象, 基于 Hyperion 数据直接反演得到的 LAI 均值约 2.06, 将数据尺度上升为 300m, 反演的 LAI 均值仅为 1.27。采用 LAI—NDVI 分析方程作为 LAI 尺度效应分析和误差纠正的基础公式, 计算 LAI 的误差纠正因子, 可以较好地实现低分辨率 LAI 反演结果的纠正。该方法可以推广到 Hyperion 数据其他分辨率下的尺度效应纠正, 也可以用于其他传感器低分辨率 LAI 产品校正, 如 MODIS 等。

(2) 分析模型的非线性和研究区景观的空间异质性对 LAI 反演尺度误差的影响, 发现模型的非线性是引起不同分辨率反演结果误差的原因之一, 但不是关键因素, 在覆盖度很低或覆盖度较高的时候可以结合具体的应用予以忽略。不同尺度 LAI 反演结果存在误差, 主要是由地表植被空间结构分布的不均匀造成, 即地表空间异质性是 LAI 反演误差的关键因素。实际上, LAI 反演尺度误差是由空间异质性结构引起的误差和算法非线性引起的误差耦合在一起造成的, 本项研究没有考虑, 有待于开展进一步的深入研究。

(3) 进一步的研究将考虑定量分析植被覆盖区内植被不同组合(玉米、小麦、其他植被)的空间异质性现象对 LAI 反演的影响, 研究建立多波段反射率 ρ 空间下的 LAI 反演误差纠正。

REFERENCES

Chen J, Ni S X and Li J J. 2006. Scaling effect and spatial variability in retrieval of vegetation LAI from remotely sensed data. *Acta Ecologica Sinica*, **26**(5): 1503—1508

Feng X M and Zhao Y S. 2005. A spectral-directional reflectance remote sensing model of the semiarid landscape. *Jounal of Remote Sensing*, **9**(4): 337—342

Garrigues S, Allard B D and Baret F. 2006. Influence of landscape spatial heterogeneity on the non-linear estimation of leaf area index from moderate spatial resolution remote sensing date. *Remote Sensing of Environment*, **105**: 286—298

Jacquemoud S and Baret F. 1990. PROSPECT: A model of leaf optical properties spectra. *Remote Sensing of Environment*, **34**:75—91

Kuusk A. 1985. The hot spot effect of a uniform vegetative cover. *Soviet Journal of Remote Sensing*, **3**(4): 645—658

Kuusk A 2001. A two-layer canopy reflectance model. *Journal of Quantitative Spectroscopy & Radiative Transfer*, **71**: 1—9

Luo Y and Su N. 2002. Selection of optimal bands from remote sensing image based on information content. *Urban Geotechnical Investigation & Surveying*. **4**(4): 28—32

Tian Y H, Woodcock C E and Wang Y J. 2002. Multi-scale analysis and validation of the MODIS LAI product, I. Uncertainty assessment. *Remote Sensing of Environment*, **83**:414—430

Tian Y H and Wang Y J. 2003. Radiative transfer based scaling of LAI retrievals from reflectance data of different resolutions. *Remote Sensing of Environment*, **84**: 143—159

Verhoef W. 1984. Light scattering by leaf layers with application to canopy reflectance modeling: the SAIL model. *Remote Sensing of Environment*, **16**: 125—141

Xu Q Z, Zhang W C, Liu S C, Zhao D Z and Jiang J J. 2003. Retrieval of leaf area index for the Heihe River watershed by using remote sensing data. *Arid Zone Research*. **20**(4): 281—285

Xu X R. 2005. Remote Sensing Physics. Beijing: Peking University Press

Xu X R, Fan W J and Tao X. 2009. The spatial scaling effect of continuous canopy Leaves Area Index retrieved by remote sensing, *Science in China*, **52**(3): 393—401

Yao Y J, Liu Q, Liu Q H and Li X W. 2007. LAI inversion uncertainties in heterogeneous surface. *Journal of Remote Sensing*. **11**(6): 763—770

Zhang R H. 1996. Experimental Remote Sensing Model and Ground Basis. Beijing: Science Press

Zhang W C, Zhong S and Hu S Y. 2008. Spatial scale transferring study on Leaf Area Index derived from remotely sensed data in the Heihe River Basin, China. *Acta Ecologica Sinica*, **28**(6): 2495—2503

Zhao Y S. 2003. Theory and Method of Remote Sensing Application and Analysis. Beijing: Science Press

附中文参考文献

陈健, 倪绍祥, 李静静. 2006. 植被叶面积指数遥感反演的尺度效应及空间变异性. 生态学报, **26**(5): 1503—1508

冯晓明, 赵英时. 2005. 半干旱草场的多角度多波段反射率遥感模型. 遥感学报, **9**(4): 337—342

罗音, 舒宁. 2002. 基于信息量确定遥感图像主要波段的方法. 城市勘测, **4**(4): 28—32

徐全芝, 张万昌, 刘三超, 赵登忠, 蒋建军. 2003. 黑河流域叶面积指数的遥感反演. 干旱区研究, **20**(4): 281—285

徐希孺. 2005. 遥感物理. 北京: 北京大学出版社

徐希孺, 范闻捷, 陶欣. 2009. 遥感反演连续植被叶面积指数的空间尺度效应. 中国科学 D 辑: 地球科学, **39**(1): 79—87

姚延娟, 刘强, 柳钦火, 李小文. 2007. 异质性地表的叶面积指数反演的不确定性分析. 遥感学报, **11**(6): 763—770

张仁华. 1996. 实验遥感模型与地面基础. 北京: 科学出版社

张万昌, 钟山, 胡少英. 2008. 黑河流域叶面积指数(LAI)空间尺度转换. 生态学报, **28**(6): 2495—2503

赵英时. 2003. 遥感应用分析原理与方法. 北京: 科学出版社